

UK/94-04
December 1994
hep-lat/9501007

Finite ma corrections for sea quark matrix elements on the lattice

J.-F. Lagaë and K.-F. Liu

*Dept. of Physics and Astronomy
Univ. of Kentucky, Lexington, KY 40506*

Abstract

We compute the ma dependence of lattice renormalization factors for sea quark matrix elements. The results differ from the $(1 + ma)$ correction factor commonly used for valence quarks and connected current insertions. We find that for sea quarks, the correction factors are in general larger and depend strongly on the Lorentz structure of the current under consideration. Results are presented both for the Wilson action and for the 2-link improved action of Hamber and Wu. Phenomenological implications are also briefly discussed in two examples.

1 Introduction

Many interesting problems in hadronic physics (e.g. the proton spin crisis, the $U(1)$ problem, the strange quark content of the nucleon, ...) require the computation of a quark current inside of a disconnected* fermionic loop. Matrix elements in the nucleon for example generally involve two types of contribution associated with the connected (fig.1.a) or disconnected (fig.1.b) insertion of the quark current. Similarly, the propagation of flavor-singlet mesons involves, besides the usual connected contribution (fig.1.c), a disconnected contribution (fig.1.d). Up to recently, only the contributions associated with fig.1.a and c (which we will call “valence” for short[†]) were considered in lattice simulations. Contributions from fig.1.b and d (which we will call “sea” for short), on the other hand, were considered too difficult to compute. Recent developments in the technology of lattice gauge theory have however made their computation feasible. Among the techniques currently being used are the Z_2 noise method [2, 3] and the non-gauge-fixed volume source technique [4, 5]. Progress is fast in this area and numerical simulations based on these methods are beginning to produce statistically significant results. It therefore becomes essential to compute the renormalization factor associated with sea quark matrix elements in order to turn the raw numbers from Monte-Carlo simulations into physical quantities. The lattice renormalization of bilinear quark operators (in the limit $ma \rightarrow 0$) was considered a long time ago [6], but the finite ma corrections were only introduced more recently [7] along with the tadpole improvement [8]. Here we would like to get a closer look at the finite ma corrections in the particular case of sea quark matrix elements. We expect this to be important for the problem at hand. One would like for example to be able to measure various strange quark matrix elements in the nucleon. In current simulations, ma is about 0.1 for a strange quark and therefore finite ma corrections might be significant in this case, and indeed they are as we will see below. At the heart of the present study is the realization that the finite ma correction factor commonly used for valence quarks and connected current insertions is not adequate for the case of sea quarks or disconnected current insertions. In section 2, we briefly review the usual approach and discuss its limitations. We also make some general comments which will be useful in understanding the results presented later. In section 3, we motivate and introduce the method that we use to compute the finite ma correction factors for sea quarks. The method in itself is rather straightforward and mostly consists in computing the perturbative response of a quark current to an external gauge field both on the lattice and in the continuum. By comparing the two results, the appropriate correction factor is then extracted. We have carried out the procedure for the scalar, pseudoscalar and axial currents which are of most direct phenomenological relevance. The computation of the relevant Feynman diagrams in the continuum is presented in section 4, whereas the lattice results are to be found in section 5. The finite ma

*Here the terms connected or disconnected refer only to the topological classification of the quark lines (regardless of the presence of gluonic lines).

[†]Actually, the connected insertions contain both valence quarks and cloud quarks and antiquarks [1].

correction factors are then computed and the results are summarized in table 1 for the Wilson action and in table 2 for the 2-link improved action of Hamber and Wu [9]. The application of these correction factors to Monte-Carlo data is discussed in section 6 for two examples (the computation of the mass of the η' and the determination of the strange quark contribution to the mass of the nucleon). In section 7, we add some final remarks and briefly discuss further developments. Our conventions and Feynman rules are presented in the appendix.

2 Wilson fermions at finite ma

It has been customary to estimate the finite ma corrections by comparing the lattice and continuum propagators of a *free quark* at $\vec{p} = 0$ [7]. The result of this computation gives a $(1 + ma)$ finite renormalization factor for quark bilinears, where ma is the mass appearing in the Lagrangian or more generally the mass obtained after tadpole improvement:

$$ma = \frac{1}{2\tilde{\kappa}} - 4 \quad \text{where} \quad \tilde{\kappa} = \kappa U_0 \simeq \frac{\kappa}{8\kappa_c} \quad (1)$$

The assumptions going into this calculation appear to be justified for valence quarks. If the quark is heavy, its 3-momentum is small and it is “almost on mass-shell”, whereas when ma goes to 0 the correction factor goes back to 1. So the approximation is reasonable for a quark propagating forward in time inside a meson or baryon at rest (although there seems to be room for improvement at small and intermediate values of ma). For sea quark matrix elements, however, the situation is completely different. Configuration by configuration, one is computing a closed quark loop in a background gauge field (see fig.1.b and d). This involves an integration over the 4-momentum of the quark running around the loop. Therefore, the kinematical restrictions (i.e. low 3-momentum and proximity to the mass-shell) which were justified for valence quarks no longer apply for sea quarks. A more general method, avoiding particular kinematical assumptions, will thus be necessary to compute the finite ma corrections in this case.

Before introducing our technique for dealing with sea quarks in section 3, we would like to make here some qualitative remarks on the nature of the problem. As is well known, the $r = 0$ theory (naive action) contains 16 fermions instead of 1 and the role of the Wilson term is to lift the degeneracy between the various species. In the limit $ma \rightarrow 0$, it does so no matter what the value of $r (\neq 0)$ is. However when ma is non-zero, the effectiveness of the Wilson term in lifting the degeneracy becomes more limited and r dependent. In this sense, at finite ma , one is dealing with an effective theory with a more complicated flavor content. There are 16 species with masses [10]:

$$\begin{array}{ccccc} ma & ma + 2r & ma + 4r & ma + 6r & ma + 8r \\ \{1\} & \{4\} & \{6\} & \{4\} & \{1\} \end{array}$$

where the degeneracy of each level is indicated between braces. It is clear that when ma becomes of the same order as r , the doublers are no longer much heavier than

the “fundamental” fermion. This causes strong lattice artifacts, in the computation of closed quark loops and requires the use of correction factors in order to map the effective “multiflavor” theory onto QCD. It is precisely the computation of these finite renormalizations that we will consider in this paper. We will see that they depend on the Lorentz structure of the current under consideration. This is to be expected. Take *naive* fermions for example, matrix elements of the scalar current in a smooth external gluonic field would be 16 times what they should be in QCD, whereas matrix elements of the axial current would be 0 in the chiral limit because the chiralities of the 16 doublers add to 0 [10]. As we will see below similar trends subsist for Wilson fermions at finite ma : matrix elements of the scalar current are overestimated whereas those of the axial current are underestimated. That is, at finite ma , the Wilson term only takes care of the doubling problem partially and this affects the measurements of sea quark matrix elements.

3 Renormalization of sea quark matrix elements

Since configuration by configuration, the computation of a sea quark matrix element reduces to the computation of an “induced quark current” in a given background gauge field, we are led to study the “response functions” to an external gluonic field. By computing the matrix element of some current in a given background gauge field on the lattice (at finite ma) and comparing with the induced current in the “same” external field in the continuum, we can estimate the lattice artifacts at this particular value of ma and correct for them. A particularly interesting example was considered by Smit and Vink several years ago [11]. They investigated the case of the flavor-singlet pseudoscalar current where a topological relation gives an exact expression for the response function. Indeed, by making use of the anomalous Ward identity

$$\partial_\mu j_{\mu 5} - 2mj_5 = 2n_f q \quad (2)$$

where q is the topological charge density defined as

$$q = \frac{1}{32\pi^2} \epsilon_{\mu\nu\rho\sigma} \text{Tr}(G_{\mu\nu} G_{\rho\sigma}) \quad (3)$$

and integrating over 4-volume, one obtains a direct relation between the zero momentum matrix element of j_5 ($Q_5 = \int d^4x j_5$) and the topological charge ($Q_t = \int d^4x q$) of the gauge field configuration:

$$mQ_5 = -n_f Q_t \quad (4)$$

It is then sufficient to take a smooth background field configuration of given topological charge on the lattice, to measure the matrix element of Q_5 at various values of ma and to compare with (4) to be able to deduce the appropriate ma dependent correction factor. We will call this factor $\kappa_P(ma)$ [P for pseudoscalar]. Smit and Vink then went on to compute the topological susceptibility through correlations of $\langle j_5(x)j_5(0) \rangle$. Taking into account the correction factor, one obtains in terms of

the lattice currents:

$$\chi = \langle Q_t^2 \rangle / V = \kappa_P^2(ma) \int d^4x \langle j_5(x)j_5(0) \rangle m^2/n_f^2 \quad (5)$$

Strictly speaking, one has to be careful at this point, since the correction factor could be gauge configuration dependent, in which case normalizing on a single configuration, as was done above, would not be adequate. However, for the present computation, a consistency check can be used to show that finite ma artifacts are to a good approximation configuration independent. We know that the topological susceptibility (being a pure glue quantity in the quenched approximation) must be independent of the mass of the quarks. An evaluation of (5) on a statistical sample of gauge configurations would however not satisfy this constraint if $\kappa_P(ma)$ wasn't the appropriate correction factor for every "important" configuration. The fact that Smit and Vink indeed obtain for (5) a mass independent result in their Monte-Carlo simulation therefore can be used as an indication that a single, configuration independent, correction factor [$\kappa_P(ma)$] is sufficient.

Now we would like to generalize the computation of finite ma corrections to other currents. The pseudoscalar current was special because of the existence of an exact "topological" relation (4); other cases won't be that straightforward. However, if we assume that the ma dependence of the correction factor is the same for all configurations (as seems to be the case from the above discussion), any background gauge field can be used for its evaluation. In particular, we can consider very weak external fields, so that perturbation theory becomes a reliable tool, and compute in this manner the relation between lattice and continuum theory. This is the strategy that we will adopt here. It turns out that the lowest order perturbative diagrams for the expectation value of a quark current $\bar{\psi}\Gamma\psi$ in an external field will be triangle diagrams like the one represented in fig.2.a . In this paper, we will restrict our attention to matrix elements of zero momentum currents (so that $q = -p$ in fig.2). This simplifies the computations and is sufficient for the applications currently envisaged ("forward" matrix elements in the nucleon, for example).

Let's consider the scalar current as an example ($\Gamma = 1$ in fig.2) . It is well known that in this case, the continuum computation of the triangle diagram, gives a relation between the matrix element of the scalar current and the square of the external field strength of momentum p (the zero momentum relation has been abundantly used in the context of QCD sum rules [12]):

$$m \langle \bar{\psi}\psi \rangle = C\left(\frac{p^2}{m^2}\right)F_{\mu\nu}^2(p) \quad (6)$$

where C is a dimensionless function of p^2/m^2 . Similarly, one can compute the triangle diagram on the lattice (see section 5 for details) and obtain the corresponding relation:

$$m \langle \bar{\psi}\psi \rangle = L(pa, ma)F_{\mu\nu}^2(p) \quad (7)$$

the only difference being that the lattice dimensionless function L can depend separately on pa and ma . The functions L and C contain all the information we need,

they tell us how the lattice and continuum scalar currents react to a given external field. By comparing the two, we can deduce which correction factor need to be introduced in lattice measurements of the scalar current. We will mostly consider the case $p=0$ (corresponding to smooth background gauge fields). Then one obtains the finite (ma dependent) renormalization factor for the scalar current:

$$\kappa_S(ma) = C(0)/L(0, ma) \quad (8)$$

Of course, one can check that $L(pa, ma)$ goes back to $C(p^2/m^2)$ when both pa and ma are small so that $\kappa_S(ma) \rightarrow 1$ when $ma \rightarrow 0$. If the numerical simulation is dominated by smooth gauge fields, then $\kappa_S(ma)$ is all that we need. However, this is not in general the case and it is therefore important to look also at the situation at finite pa . To investigate this momentum dependence, we will present below comparative plots of $L(pa, ma)$ and $C((pa)^2/(ma)^2)$ at fixed values of ma . The perturbative method presented here for the scalar current generalizes, mutatis mutandis, to other currents. One can for example compute the finite ma correction factor for the pseudoscalar current and then compare with the topological charge method presented earlier. The two results agree provided that the “instanton” field is weak enough.

A general remark is in order here. In the case of valence quarks [7, 8], it is assumed that the ma and β (or α_s) dependence of the renormalization factor factorize:

$$Z = 2\tilde{\kappa}(1 + ma)[1 + O(\alpha_V)] \quad (9)$$

We make the same factorization hypothesis here. This is what allows the computation of the ma dependence at lowest non-trivial order in perturbation theory. The actual order at which the computation is done however differs for valence and sea quarks. In the valence case, the ma dependence is computed for a free quark. For the correlation between two closed quark loops (fig.1.d), on the other hand, the lowest non-trivial order is α_s^4 [or α_s^2 for a single quark loop in a background field]. This is why for sea quarks, we extract the ma dependence from the triangle diagram (fig.2). So that in summary, given the factorization hypothesis, what we compute here for sea quarks is the factor replacing the $(1 + ma)$ factor of valence quarks; the rest of the renormalization factor ($[1 + O(\alpha_V)]$ and tadpole corrections) remains unchanged. Another way to look at this factorization for sea quarks would be to view the gauge field configurations as a smooth background field with additional short wavelength fluctuations. In this picture, the ma dependent factor corrects the response to the smooth background field and the perturbative factor accounts for the short wavelength fluctuations.

4 Response to continuum background fields

The continuum computation of diagrams like the one presented in fig.2.a is rather straightforward. The Feynman rules that we have used are presented in the appendix. These diagrams are finite and the only subtlety in their computation is the introduction of a Pauli-Villars regulator (which simply consists in subtracting the same

fermionic loop for an infinitely heavy quark) to ensure gauge invariance. We have done the computation for the axial, scalar and pseudoscalar currents ($\Gamma = \gamma_\alpha \gamma_5, \gamma_5$ and I respectively) which are of most direct phenomenological relevance. As mentioned above, we will restrict our attention to zero momentum currents so that $q = -p$ in fig.2 . For the pseudoscalar current, however, this would lead to a vanishing result and we therefore give the general formula in this case. Finally, we should mention that when quoting our final results, we consider not only the diagram of fig.2.a, but the sum of this diagram and the one with crossed photon legs [fig.2.b] (We do not include the external gauge fields and couplings in our expressions, since they are just common factors which can be brought back at the end). This gives us respectively, for the axial current ($q = -p$):

$$A_{\alpha\mu\nu}(p, -p) = -\frac{1}{\pi^2} \epsilon_{\mu\nu\alpha\beta} p_\beta A\left(\frac{p^2}{m^2}\right) \quad (10)$$

for the scalar current ($q = -p$):

$$S_{\mu\nu}(p, -p) = \frac{1}{6\pi^2 m} (\delta_{\mu\nu} p^2 - p_\mu p_\nu) S\left(\frac{p^2}{m^2}\right) \quad (11)$$

and for the pseudoscalar current:

$$P_{\mu\nu}(p, q) = \frac{1}{8\pi^2 m} \epsilon_{\mu\nu\alpha\beta} q_\alpha p_\beta P\left(\frac{p^2}{m^2}, \frac{q^2}{m^2}, \frac{p \cdot q}{m^2}\right) \quad (12)$$

where the functions A,S,P are given by:

$$A\left(\frac{p^2}{m^2}\right) = \frac{1}{2} \left\{ 1 - \frac{m^2}{p^2} \frac{1}{\sqrt{}} \ln\left(\frac{\sqrt{} + 1/2}{\sqrt{} - 1/2}\right) \right\} \quad (13)$$

$$S\left(\frac{p^2}{m^2}\right) = 12 \left(\frac{m^2}{p^2}\right) A\left(\frac{p^2}{m^2}\right) \quad (14)$$

$$P\left(\frac{p^2}{m^2}, \frac{q^2}{m^2}, \frac{p \cdot q}{m^2}\right) = \int_0^1 dx \int_0^{1-x} dy \frac{2m^2}{q^2 x(1-x) + p^2 y(1-y) + 2p \cdot qxy + m^2} \quad (15)$$

with

$$\sqrt{} = \sqrt{\frac{1}{4} + \frac{m^2}{p^2}} \quad (16)$$

Note that all these expressions lead to gauge invariant results (even for the axial current since $q = -p$). Finally, by using the asymptotic expansion of the functions A, S and P, one obtains the low momentum limits of (10), (11) and (12):

$$A_{\alpha\mu\nu}(p, -p) \xrightarrow{p \rightarrow 0} -\frac{1}{12\pi^2} \epsilon_{\mu\nu\alpha\beta} p_\beta \frac{p^2}{m^2} \quad (17)$$

$$S_{\mu\nu}(p, -p) \xrightarrow{p \rightarrow 0} \frac{1}{6\pi^2 m} (\delta_{\mu\nu} p^2 - p_\mu p_\nu) \quad (18)$$

$$P_{\mu\nu}(p, q) \xrightarrow{p, q \rightarrow 0} \frac{1}{8\pi^2 m} \epsilon_{\mu\nu\alpha\beta} q_\alpha p_\beta \quad (19)$$

We should mention that all the diagrams have been computed for QED rather than QCD. This doesn't affect the comparison between lattice and continuum at lowest order in perturbation theory and avoids the unnecessary burden of carrying color factors all the way through the computation. In fact, once the matrix element of a local fermionic current has been computed at lowest order in an external QED field and expressed in gauge invariant terms, the result can be generalized immediately to QCD (Color factors have to be added but there is no need to compute explicitly the 3 or 4 external gluon lines diagram which are required to insure gauge invariance in QCD).

5 Lattice results and finite ma correction factors

We now want to compute the perturbative “response functions” on the lattice in order to compare them with the continuum results presented above. The computation will be done both for the Wilson action and for the 2-link improved action of Hamber and Wu (see appendix for our conventions and Feynman rules). As before, the actual calculations will be carried out in the context of QED. Lattice perturbation theory is characterized in general by the appearance of new Feynman diagrams with “multi-photon” vertices. In our case, the “fish diagram” (fig.2.c) appears in addition to the two triangle diagrams (fig.2.a and b). The lattice expression for diagrams of the type of figure 2.a is:

$$I_{\mu\nu}^\Gamma(p, q) = \int \frac{d^4 k}{(2\pi)^4} \text{Tr} [\Gamma S_F(k - q) \Gamma_\nu(k, -q) S_F(k) \Gamma_\mu(k, p) S_F(k + p)] \quad (20)$$

where the integral over k extends from $-\pi$ to $+\pi$ in each direction and the vertex Γ_μ and propagator S_F are defined in the appendix. The expression for the diagram of fig.2.b can be obtained directly from (20) by the exchange $p, \mu \leftrightarrow q, \nu$. Finally, the fish diagram fig.2.c gives the integral

$$J_{\mu\nu}^\Gamma(p, q) = \int \frac{d^4 k}{(2\pi)^4} \text{Tr} [\Gamma S_F(k - q) \Gamma_{\mu\nu}^{(2)}(k + p, -p, -q) S_F(k + p)] \quad (21)$$

where $\Gamma_{\mu\nu}^{(2)}$ is defined in the appendix (eq.(37)).

Let's begin by describing the computation for the pseudoscalar current which is probably the simplest of all. Note that in this case ($\Gamma = \gamma_5$) the trace in (21) vanishes so that only the integral (20) has to be computed. Replacing Γ by γ_5 , using the formulas (36) and (38) in the Appendix, and taking the Dirac trace, we get:

$$I_{\mu\nu}^5(p, q) = \int \frac{d^4 k}{(2\pi)^4} \frac{1}{Z(k - q)Z(k)Z(k + p)} \{4\epsilon_{\mu\nu\beta\delta} V_\mu(k, p) V_\nu(k, -q) M(k - q) S_\beta(k) S_\delta(k + p)\}$$

$$\begin{aligned}
& -4\epsilon_{\mu\nu\beta\delta}V_\mu(k+p)V_\nu(k,-q)M(k)S_\beta(k-q)S_\delta(k+p) \\
& +4\epsilon_{\mu\nu\beta\delta}V_\mu(k+p)V_\nu(k,-q)M(k+p)S_\beta(k-q)S_\delta(k) \\
& -4r\epsilon_{\mu\alpha\beta\delta}V_\mu(k,p)W_\nu(k,-q)S_\alpha(k-q)S_\beta(k)S_\delta(k+p) \\
& -4r\epsilon_{\alpha\nu\beta\delta}W_\mu(k,p)V_\nu(k,-q)S_\alpha(k-q)S_\beta(k)S_\delta(k+p)
\end{aligned} \tag{22}$$

The integral over d^4k can then be carried out numerically for the Wilson or the improved action by using the explicit expression given in the appendix for the various functions S,M,Z,V,W. However, since we are mostly interested in the case of small momenta ($p, q \rightarrow 0$), it is interesting to go one step further in the analytical evaluation and carry out the Taylor expansion of (22) up to second order in p and q . This computation is simplified by the fact that only the numerator needs to be expanded to second order (it turns out that the terms coming from the expansion of the denominator vanish because of the antisymmetry of the ϵ symbol). The final result for Wilson fermions is ($p, q \rightarrow 0$):

$$I_{\mu\nu}^5(p, q) = 4\epsilon_{\mu\nu\alpha\beta}q_\alpha p_\beta \int \frac{d^4k}{(2\pi)^4} \frac{1}{Z^3(k)} \left(\prod_{\rho=1}^4 \cos k_\rho \right) \left[M(k) - r \sum_\lambda \frac{\sin^2 k_\lambda}{\cos k_\lambda} \right] \tag{23}$$

And for the 2-link improved action, we have:

$$I_{\mu\nu}^5(p, q) = 4\epsilon_{\mu\nu\alpha\beta}q_\alpha p_\beta \int \frac{d^4k}{(2\pi)^4} \frac{1}{Z^3(k)} \left(\prod_{\rho=1}^4 C_\rho(k) \right) \left[M(k) - r \sum_\lambda \frac{S_\lambda(k)}{C_\lambda(k)} T_\lambda(k) \right] \tag{24}$$

where we have introduced:

$$C_\lambda(k) = \frac{1}{3}(4 \cos k_\lambda - \cos 2k_\lambda) \tag{25}$$

$$T_\lambda(k) = \frac{1}{3}(4 \sin k_\lambda - 2 \sin 2k_\lambda) \tag{26}$$

The integrals in (23) and (24) were evaluated numerically by using a trapezoidal rule on a non-uniform grid. The resolution was chosen to be maximum around $k = 0$ where the integrand peaks (especially when ma is small). In practice, we mostly used a set of nested $(4)^4$ grids where at each step, the resolution is increased by a factor of 2 in the inner portion of the grid (see fig.3 for an example). In order to control the discretization errors, we further varied the resolution on each of the embedded grids separately and checked for convergence. The nesting procedure is stopped when the contribution from the inner grid becomes smaller than the overall discretization error. In practice, 10 levels of nesting or less were always sufficient. Once the numerical integrals have been computed, we can sum the contributions from the diagrams of fig.2 and compare the result with the continuum formula (19). In figure 4, we plot the ratio of the lattice to the continuum results for the Wilson and improved action as a function of ma (at $r = 1$). All curves agree at $ma = 0$ (as they should), but it is clear that elsewhere, Wilson fermions strongly underestimate the matrix elements of the pseudoscalar current. The situation is significantly improved in the case of the 2-link

action. These results are in agreement with those of Hamber and Wu [9] and Smit and Vink [11]. In tables 1 and 2, we collect the finite renormalization factors to be used in lattice simulations of sea quark matrix elements (inverse of the quantities plotted in fig. 4). We do so for the range of masses $0 < ma < 0.2$ relevant for current simulations and including the mass of the strange quark. The precision on these renormalization factors is always better than 1%. For comparison, we also include the corresponding factors for valence Wilson quarks $(1 + ma)$. We would like to remind the reader that the numbers presented in tables 1 and 2 represent only the ma dependent part of the renormalization factors, the usual perturbative renormalization factors have to be included separately.

Let's now consider the case of the axial current. We have to compute (20) and (21) with Γ replaced by $i\gamma_\alpha\gamma_5$ [i is added in order to get a real answer]. Taking the trace directly in (20) would however lead to a rather lengthy expression. We will therefore restrict our attention to the case $q = -p$, which is sufficient for our purposes [zero momentum matrix elements of $j_{\alpha 5}$]. Note that for $q = -p$, the fish diagram for the axial current [(21) with Γ replaced by $i\gamma_\alpha\gamma_5$] will vanish by the antisymmetry of the ϵ symbol. For (20) we then obtain:

$$\begin{aligned}
I_{\mu\nu}^{\alpha 5}(p, -p) &= \int \frac{d^4k}{(2\pi)^4} \frac{1}{Z^2(k)Z(k+p)} \\
&4\left\{\frac{1}{2}\epsilon_{\lambda\mu\nu\delta}V_\mu(k,p)V_\nu(k,p)[2S_\delta(k)D(k,k+p) - S_\delta(k+p)Z(k)]\right. \\
&-2\epsilon_{\lambda\mu\beta\delta}V_\mu(k,p)V_\nu(k,p)S_\beta(k+p)S_\delta(k)S_\nu(k) \\
&-2\epsilon_{\lambda\mu\beta\delta}V_\mu(k,p)W_\nu(k,p)rM(k)S_\beta(k+p)S_\delta(k) \\
&\left.-(\mu \leftrightarrow \nu)\right\}
\end{aligned} \tag{27}$$

where we have introduced:

$$D(k, k+p) = \sum_{\alpha} S_{\alpha}(k)S_{\alpha}(k+p) + M(k)M(k+p) \tag{28}$$

As in the pseudoscalar current case, one could in principle expand the integral in powers of p . However this is rather difficult in the present case. One can show for example that the lowest non-trivial order is $O(p^3)$. Order 0 and 2 vanish by symmetrical integration and order one is a total divergence. Therefore, the expansion appears rather complicated and not really interesting given that the final integration will be computed numerically anyway. We therefore opted for the numerical computation of (27) at various values of p and an extrapolation to $p = 0$. The numerical integration proceeds as before except that now, there are 2 points where the integrand peaks ($k = 0$ and $k = -p$). We take this into account by refining the grid separately around these 2 points. Our integration routine generates the grids and does all the bookkeeping automatically. The procedure is in fact rather general and is in a sense a restriction of the adaptative quadrature method to the case where the position of "troublesome" points is known in advance. Discretization errors are controlled as before by doubling the resolution on each of the nested grids separately. For small

momentum, the results of the numerical integration can be compared with the continuum formula (17). The inverse ratio $1/\kappa_A$ is plotted in fig.5 and the axial correction factor κ_A presented in tables 1 and 2. The results are qualitatively similar to those obtained for j_5 except that the lattice artifacts are smaller for the axial than for the pseudoscalar current. Finally, it is also interesting to look at the situation at finite pa as this might become useful in a more thorough analysis of lattice artifacts. That is, although we would hope that a numerical simulation is dominated by gluonic fields of small pa , we have no reason to assume this a priori and it might be important to look at “rough” fields too. We would therefore like to fix ma and compare the momentum dependence of the lattice integrals with the continuum formula (10). In fig.6, we present the result of such a comparison with ma fixed at 0.2 (the continuum solid curve corresponds to $A(p^2/m^2)$ as given by (13) and the dots are results obtained on a grid of lattice momenta). We have limited the comparison to the range $|pa| \leq 2\pi$ accessible on the lattice.

Finally, let’s consider the scalar current. Note that in this case, the “fish” diagram (fig.2.c) is non-zero and has to be included as well. Only the sum of all 3 diagrams in fig.2 gives a gauge invariant result. In fact, we checked that the final results obtained in this way are proportional to a lattice transverse tensor which reduces to $(\delta_{\mu\nu} - p_\mu p_\nu/p^2)$ in the low momentum limit. In our most extensive comparisons between lattice and continuum, however, we didn’t compute the full tensor but rather focused our attention on a single off-diagonal element. The fish diagram, being proportional to $\delta_{\mu\nu}$, doesn’t appear in this case and this helps in further reducing the computer time requirements. The expression for the triangle diagram (20) with $\Gamma = 1$ and $q = -p$ is:

$$\begin{aligned}
I_{\mu\nu}(p, -p) = & \int \frac{d^4k}{(2\pi)^4} \frac{1}{Z^2(k)Z(k+p)} \\
& \{V_\mu(k,p)V_\nu(k,p)8M(k) [S_\mu(k+p)S_\nu(k) + S_\mu(k)S_\nu(k+p)] \\
& +4rV_\mu(k,p)W_\nu(k,p) [2M(k)F_\mu(k,k+p) - S_\mu(k+p)Z(k)] \\
& +4rW_\mu(k,p)V_\nu(k,p) [2M(k)F_\nu(k,k+p) - S_\nu(k+p)Z(k)] \quad (29) \\
& -4r^2W_\mu(k,p)W_\nu(k,p) [2M(k)E(k,k+p) + M(k+p)Z(k)] \\
& -4\delta_{\mu\nu} [V_\mu(k,p)]^2 [2M(k)D(k,k+p) - M(k+p)Z(k)]\}
\end{aligned}$$

where we have introduced:

$$E(k, k+p) = \sum_{\alpha} S_{\alpha}(k)S_{\alpha}(k+p) - M(k)M(k+p) \quad (30)$$

$$F_{\mu}(k, k+p) = S_{\mu}(k)M(k+p) + S_{\mu}(k+p)M(k) \quad (31)$$

The numerical integration of (29) proceeds as in the case of the axial current. The computations are made for various values of p and extrapolated down to $p = 0$. Comparing the small momentum lattice results with the continuum formula (18) gives the renormalization factor $\kappa_S(ma)$ defined in (8). The inverse of this factor is plotted in fig.7. It appears that when ma is non-zero and moderate, Wilson fermions

overestimate the continuum result. The deviation is significant, being almost 30% at $ma = 0.1$. (The renormalization factor is tabulated in table 1). At large values of ma on the other hand, the lattice would underestimate the continuum result. The Hamber-Wu action provides a moderate improvement for small values of ma . However for $ma \geq 0.1$, the situation is as bad or even worse than for Wilson fermions (The correction factors for the improved action are given in table 2). We also made a comparison of lattice and continuum results at finite momentum. By fixing $ma = 0.2$, we obtain the results presented in figure 8. The continuum solid curve corresponds to the function $S(p^2/m^2)$ as given by (14). Note that up to an overall factor, this is precisely the comparison between the functions L and C [eqs. (6) and (7)] introduced in section 3 [eq. (11) provides the exact correspondence]. From the curves of figure 8, it appears that for background fields of non-zero momentum, Wilson fermions overestimate matrix elements of the scalar current even more than in the zero momentum limit. It is interesting to contrast this with what happens in the case of naive fermions (There of course, one divides the lattice results by 16 before making the comparison with the continuum). The results are presented in fig.9 and turn out to be much better than for the Wilson case. It is not entirely clear what the origin of the problem is with Wilson fermions. They probably essentially come from the form of the quark-gluon vertex [i.e. eq.(36)]. Gluons do not only couple to the quarks through γ_μ but also directly through a “mass term” rW_μ . In fact, one can check that by artificially truncating the vertex (taking $r = 0$ in (36)) in the Wilson fermion calculation of the triangle diagram and leaving the propagators unchanged, one obtains a result very similar to fig.9. The result of fig.8 indicates that one has to be very careful when using Wilson fermions to measure matrix elements of the scalar current on the lattice. Simulation results might be even more overestimated than we would think from the low momentum analysis given above and leading to the scalar correction factors given in table 1. This will have to be analyzed in more detailed investigations.

6 Examples of phenomenological applications

The results presented above indicate that the finite ma correction factors for sea quarks are in general rather large and will therefore strongly influence the interpretation of simulation results. To illustrate this, we now discuss their application to two interesting problems [13]. The first is the computation of the mass shift of the η' . In a quenched simulation, it can be estimated from a measurement of the coupling between the would be Goldstone bosons. The computation involves the ratio of a 2-loop (fig.1.d) to 1-loop (fig.1.c) amplitude [4]. As a consequence of the above discussion, we expect that they will have different renormalization factors: The 1-loop part behaves as a “valence” quark and will therefore pick-up a $(1 + ma)$ correction for each current whereas the 2-loop diagram corresponds to a “sea” quark situation, in which case, the pseudoscalar factor of table 1 is relevant. In figure 10, we compare the mass of the η' after correction with the raw lattice data [4]. The trends are very

different: after correction, the mass shift of the η' is essentially independent of the mass of the quark up to the strange quark mass with a chiral limit that is in much better agreement with the estimate obtained from the Witten-Veneziano formula (We assume that the drop in the renormalized data at the lowest quark mass can be attributed to finite size effects or to the zero-mode shift effect [11]). The agreement between the renormalized data and the Witten-Veneziano estimate $M_0^2 = 2N_f\chi/f_\pi^2$ doesn't come as a surprise, since the correction factor that we are advocating here is the same as the one used by Smit and Vink [11] to compute the topological susceptibility by the fermionic method [See eq.(5)]. It is just a matter of self-consistency that the correction factor appearing in (5) be used as well in the computation of the 2-loop amplitude [Fig.1.d] as a function of time separation. Otherwise, the Witten-Veneziano relation could not be recovered on the lattice. Note also that the (quark) mass independence of the coupling between the would be Goldstone bosons is a basic assumption in the Witten-Veneziano mass formula. It is nice to be able to verify it on the lattice. As a second example, we mention the contribution of the strange quark to the mass of the nucleon. If we replace the $(1 + ma)$ correction factor used in [5] with the sea quark scalar correction factor from table 1, we find that the strange quark contribution to the mass of the nucleon comes down, from 30% to 21% - a change of 30%.

7 Conclusions

We have computed the ma dependent part of lattice renormalization factors for sea quark matrix elements. The results depend strongly on the Lorentz structure of the current under consideration. This is unlike the valence quark situation where in first approximation, a single ma dependent correction factor can be used for all currents. We found for example that for Wilson fermions, sea quark matrix elements of the axial and pseudoscalar current are underestimated whereas those of the scalar current are overestimated. The perturbative method that we have used for computing the finite ma correction factors is general and could be used for other local currents, as well as for point-split currents. The ma dependent corrections for sea quarks are rather large and generally dominate the remaining part of the renormalization factor ($2\tilde{\kappa}[1 + O(\alpha_V)]$), which of course underlies their phenomenological importance. In section 6, we applied our renormalization factors to the results of recent lattice simulations concerning the mass shift of the η' [4] and the strange quark content of the nucleon [5]. In both cases, it was found that the finite ma correction had a large impact and helped in bringing the simulation result closer to phenomenological estimates.

There is also much interest in trying to reduce the magnitude of these correction factors by using modified actions. Our results for the axial and pseudoscalar currents for example give a strong motivation for using the 2-link improved action of Hamber and Wu in these cases. For the scalar current, on the other hand, this kind of improvement doesn't seem to help much and it is probably more interesting to consider

other alternatives, such as staggered fermions for example or working with naive fermions and dividing the result by 16. Finally, we would like to recall that the renormalization factors quoted in tables 1 and 2 have been obtained assuming that the lattice simulation is dominated by low momentum gauge fields. What happens exactly in more general situations will have to be investigated in later studies. In the final analysis, it seems to us that the ideas presented here would be best tested by doing simulations using different actions (Wilson versus improved for example or Wilson at different values of r), applying the appropriate correction factor in each case and then checking the overall compatibility of the physical results.

8 Appendix

The action for Wilson and two-link improved fermions is usually defined as [9]:

$$\begin{aligned}
A_F &= \kappa \sum_{n,\mu} \left[\bar{\psi}_n(r - \gamma_\mu) U_{n,\mu} \psi_{n+\mu} + \bar{\psi}_{n+\mu}(r + \gamma_\mu) U_{n,\mu}^\dagger \psi_n \right] \\
&+ \sum_{n,\mu} \left[\bar{\psi}_n(C - D\gamma_\mu) U_{n,\mu} U_{n+\mu,\mu} \psi_{n+2\mu} + \bar{\psi}_{n+2\mu}(C + D\gamma_\mu) U_{n+\mu,\mu}^\dagger U_{n,\mu}^\dagger \psi_n \right] \\
&- \sum_n \bar{\psi}_n \psi_n
\end{aligned} \tag{32}$$

For the Wilson action, $C = D = 0$; whereas for the improved action, C and D are chosen to cancel all terms of order $(pa)^2$ and $(pa)^3$ in the expansion of the action. One then finds:

$$C = \frac{-\kappa r}{4} \quad D = \frac{-\kappa}{8} \tag{33}$$

It has to be remarked, however, that with this definition, the 0^{th} order term and the terms linear in (pa) are modified by the improvement procedure. This is usually corrected at the end of the computation by introducing a wave function renormalization and by changing the definition of the quark mass in terms of κ ($ma = \frac{2}{3\kappa} - 4r$). Here however, we will choose the alternative solution of making the correction from the start. That is, in the *improved* case, we will multiply the action (32) by $4/3$. This will insure that our Feynman rules have the correct continuum (=low momentum) limit. In this way, the relation between ma and κ will also be the same for the two actions:

$$ma = \frac{1}{2\kappa} - 4r \tag{34}$$

Finally, in the same spirit of keeping things as close as possible to the continuum formulation, we absorb the factor of $\sqrt{2\kappa}$ in the definition of ψ . With these remarks, we can now introduce our Feynman rules. Our definitions are the same as in [14]. We write the inverse fermion propagator in the form:

$$S_F^{-1}(p) = \sum_\alpha i\gamma_\alpha S_\alpha(p) + M(p) \tag{35}$$

the 1-photon vertex (fig.11.a) in the form:

$$\Gamma_\mu(k, q) = i\gamma_\mu V_\mu(k, q) + rW_\mu(k, q) \quad (36)$$

and the 2-photon vertex (fig.11.b) in the form:

$$\Gamma_{\mu\nu}^{(2)}(k, q, p) = \delta_{\mu\nu} \left(i\gamma_\mu V_\mu^{(2)}(k, q, p) - rW_\mu^{(2)}(k, q, p) \right) \quad (37)$$

From (35), we find for the fermion propagator:

$$S_F(p) = \frac{-i \sum_\alpha \gamma_\alpha S_\alpha(p) + M(p)}{Z(p)} \quad (38)$$

where we have defined

$$Z(p) = \sum_\beta S_\beta^2(p) + M^2(p) \quad (39)$$

We then have for Wilson fermions:

$$S_\alpha(p) = \sin p_\alpha \quad (40)$$

$$M(p) = m + 4r - r \sum_\beta \cos p_\beta \quad (41)$$

$$V_\mu(k, q) = \cos(k_\mu + \frac{q_\mu}{2}) \quad (42)$$

$$W_\mu(k, q) = \sin(k_\mu + \frac{q_\mu}{2}) \quad (43)$$

$$V_\mu^{(2)}(k, q, p) = \sin(k_\mu + \frac{q_\mu}{2} + \frac{p_\mu}{2}) \quad (44)$$

$$W_\mu^{(2)}(k, q, p) = \cos(k_\mu + \frac{q_\mu}{2} + \frac{p_\mu}{2}) \quad (45)$$

and for the improved action:

$$S_\alpha(p) = \frac{1}{6}(8 \sin p_\alpha - \sin 2p_\alpha) \quad (46)$$

$$M(p) = m + 4r - \frac{r}{3} \sum_\beta (4 \cos p_\beta - \cos 2p_\beta) \quad (47)$$

$$V_\mu(k, q) = \frac{1}{3} \left[4 \cos(k_\mu + \frac{q_\mu}{2}) - \cos(\frac{q_\mu}{2}) \cos(2k_\mu + q_\mu) \right] \quad (48)$$

$$W_\mu(k, q) = \frac{1}{3} \left[4 \cos(k_\mu + \frac{q_\mu}{2}) - 2 \cos(\frac{q_\mu}{2}) \sin(2k_\mu + q_\mu) \right] \quad (49)$$

$$V_\mu^{(2)}(k, q, p) = \frac{1}{3} \left[4 \sin(k_\mu + \frac{q_\mu}{2} + \frac{p_\mu}{2}) - 2 \cos(\frac{q_\mu}{2}) \cos(\frac{p_\mu}{2}) \sin(2k_\mu + q_\mu + p_\mu) \right] \quad (50)$$

$$W_\mu^{(2)}(k, q, p) = \frac{1}{3} \left[4 \cos(k_\mu + \frac{q_\mu}{2} + \frac{p_\mu}{2}) - 4 \cos(\frac{q_\mu}{2}) \cos(\frac{p_\mu}{2}) \cos(2k_\mu + q_\mu + p_\mu) \right] \quad (51)$$

In writing these Feynman rules, we have omitted all the factors of the lattice spacing a . These however are obvious on dimensional grounds and can easily be reinstated at the end of the computation if necessary. Finally, the continuum Feynman rules are obtained straightforwardly by taking the low momentum limit of the above formulas. The result is:

$$S_\alpha(p) = p_\alpha \quad M(p) = m \quad V_\mu = 1 \quad W_\mu = V_\mu^{(2)} = W_\mu^{(2)} = \dots = 0 \quad (52)$$

References

- [1] K.-F. Liu and S.-J. Dong, Phys. Rev. Lett. 72, 1790 (1994)
- [2] S.-J. Dong and K.-F. Liu, Phys. Lett. B328, 130 (1994)
- [3] S.-J. Dong and K.-F. Liu, $\pi N\sigma$ Term and Quark Spin Content of the Nucleon, UK/94-07 (hep-lat/9412059)
- [4] Y. Kuramashi, M. Fukugita, H. Mino, M. Okawa and A. Ukawa, Phys. Rev. Lett. 72, 3448 (1994)
- [5] M. Fukugita, Y. Kuramashi, M. Okawa and A. Ukawa, Pion-Nucleon sigma term in lattice QCD, UTHEP-281, hep-lat/9408002
- [6] G. Martinelli and Y.-C. Zhang, Phys. Lett. B123, 433(1983); B125,77(1983)
- [7] G.P. Lepage, Nucl. Phys. B (Proc. Suppl.) 26 (1992) 45; A.S. Kronfeld, Nucl. Phys. B (Proc.Suppl.) 30 (1993) 445
- [8] G.P. Lepage and P. Mackenzie, Phys. Rev. D48 (1993) 2250
- [9] H.W.Hamber and C.M.Wu, Phys. Lett. 136B, 255 (1984)
- [10] L.H. Karsten and J.Smit, Nucl. Phys. B183 (1981) 103
- [11] J. Smit and J.C. Vink, Nucl. Phys. B286 (1987) 485, B307 (1988) 549; Phys. Lett. B194, 433 (1987)
- [12] M.A. Shifman, A.I. Vainshtein and V.I. Zakharov, Nucl. Phys. B147 (1979) 385, 448, 519
- [13] J.-F. Lagaë and K.-F. Liu, Finite ma corrections for sea quark matrix elements, UK/94-05, hep-lat/9412023, To appear in the proceedings of the LATTICE'94 conference, Nucl. Phys. B (Proc. Suppl. section)
- [14] C. Bernard, A. Soni and T. Draper, Phys. Rev. D36, 3224 (1987)

Table Caption

1. ma dependence of local “sea” currents renormalization factors for Wilson fermions ($r=1$).
2. Same as table 1 for Hamber-Wu fermions.

Figure Caption

1. Quark skeleton diagrams associated with various measurements: (a) Connected and (b) disconnected contributions to a matrix element in the nucleon. (c) Connected and (d) disconnected contributions to the propagator of a flavor-singlet meson.
2. Leading order diagrams contributing to the matrix element of a current in an external field (Diagram (c) appears only on the lattice).
3. Example of a grid used for numerical integration.
4. Pseudoscalar current response to a given external field. The ratio of the lattice and continuum responses is plotted versus ma for two choices of the lattice action.
5. Same as fig.4 for the axial current.
6. Dependence of the axial current response function on the momentum of the external gauge field (ma is fixed at 0.2 and pa varies between 0 and 2π). The continuum response function (solid line) is included for comparison.
7. Same as fig.4 for the scalar current.
8. Same as fig.6 for the scalar current.
9. Same as fig.8 for naive fermions (after division by 16).
10. η' mass shift vs quark mass after renormalization (squares) and before (plusses). Also included are the chiral extrapolation of the raw data (diamond) and the estimate from the Witten-Veneziano formula (circle), using the topological susceptibility χ obtained in [4].
11. One and two photon vertices.

ma	valence quarks	sea quarks		
		pseudoscalar (κ_P)	axial (κ_A)	scalar (κ_S)
0.00	1.00	1.000	1.000	1.000
0.02	1.02	1.199	1.045	0.865
0.04	1.04	1.373	1.093	0.816
0.06	1.06	1.550	1.146	0.795
0.08	1.08	1.732	1.204	0.787
0.10	1.10	1.922	1.265	0.787
0.12	1.12	2.121	1.329	0.793
0.14	1.14	2.331	1.397	0.803
0.16	1.16	2.552	1.467	0.816
0.18	1.18	2.784	1.542	0.832
0.20	1.20	3.029	1.619	0.849

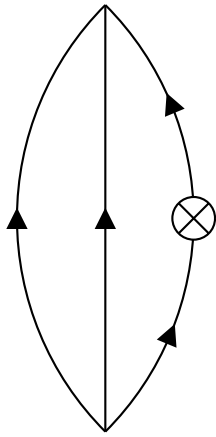
Table 1

ma	sea quarks		
	pseudoscalar (κ_P)	axial (κ_A)	scalar (κ_S)
0.00	1.000	1.000	1.000
0.02	1.038	1.000	0.946
0.04	1.078	1.001	0.894
0.06	1.120	1.004	0.852
0.08	1.165	1.007	0.816
0.10	1.212	1.012	0.784
0.12	1.261	1.018	0.758
0.14	1.312	1.026	0.735
0.16	1.366	1.034	0.715
0.18	1.422	1.044	0.697
0.20	1.480	1.055	0.682

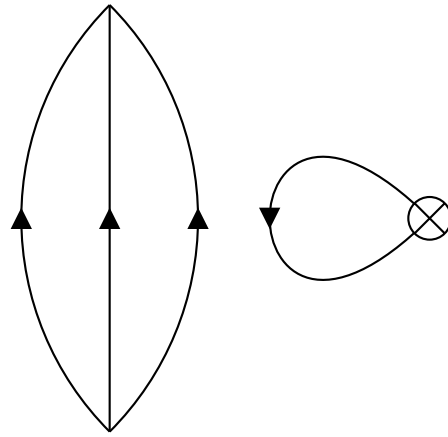
Table2

This figure "fig1-1.png" is available in "png" format from:

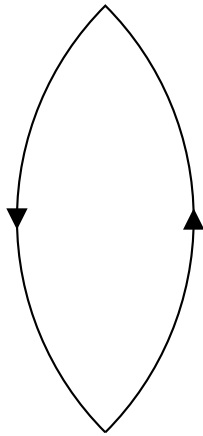
<http://arxiv.org/ps/hep-lat/9501007v1>



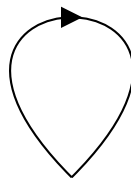
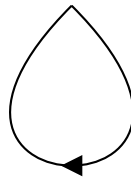
(a)



(b)



(c)



(d)

Fig. 1

This figure "fig1-2.png" is available in "png" format from:

<http://arxiv.org/ps/hep-lat/9501007v1>

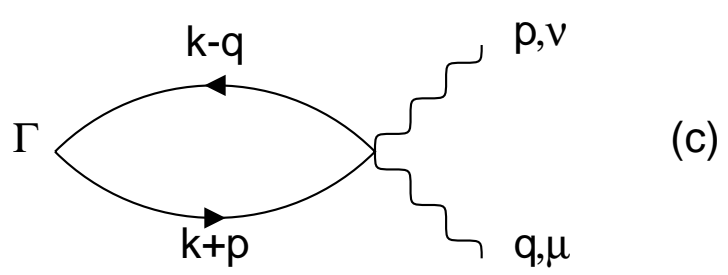
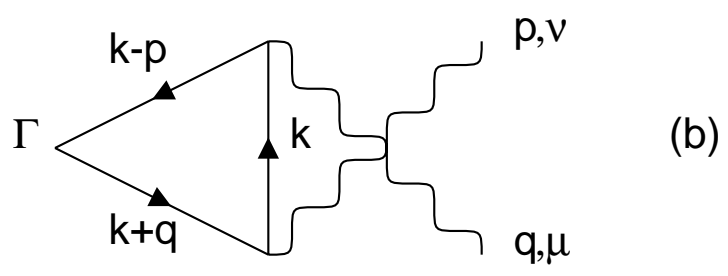
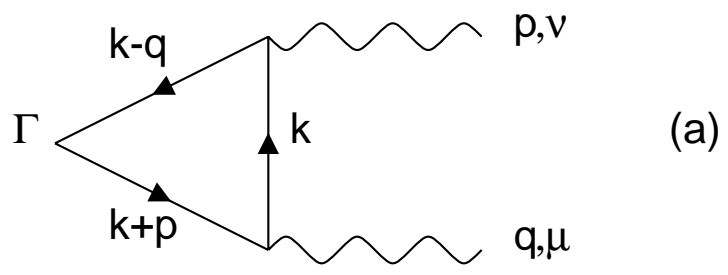


Fig. 2

This figure "fig1-3.png" is available in "png" format from:

<http://arxiv.org/ps/hep-lat/9501007v1>

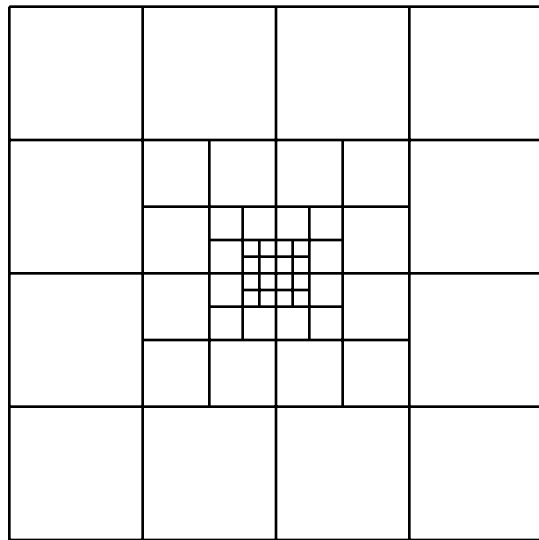


Fig. 3

This figure "fig1-4.png" is available in "png" format from:

<http://arxiv.org/ps/hep-lat/9501007v1>

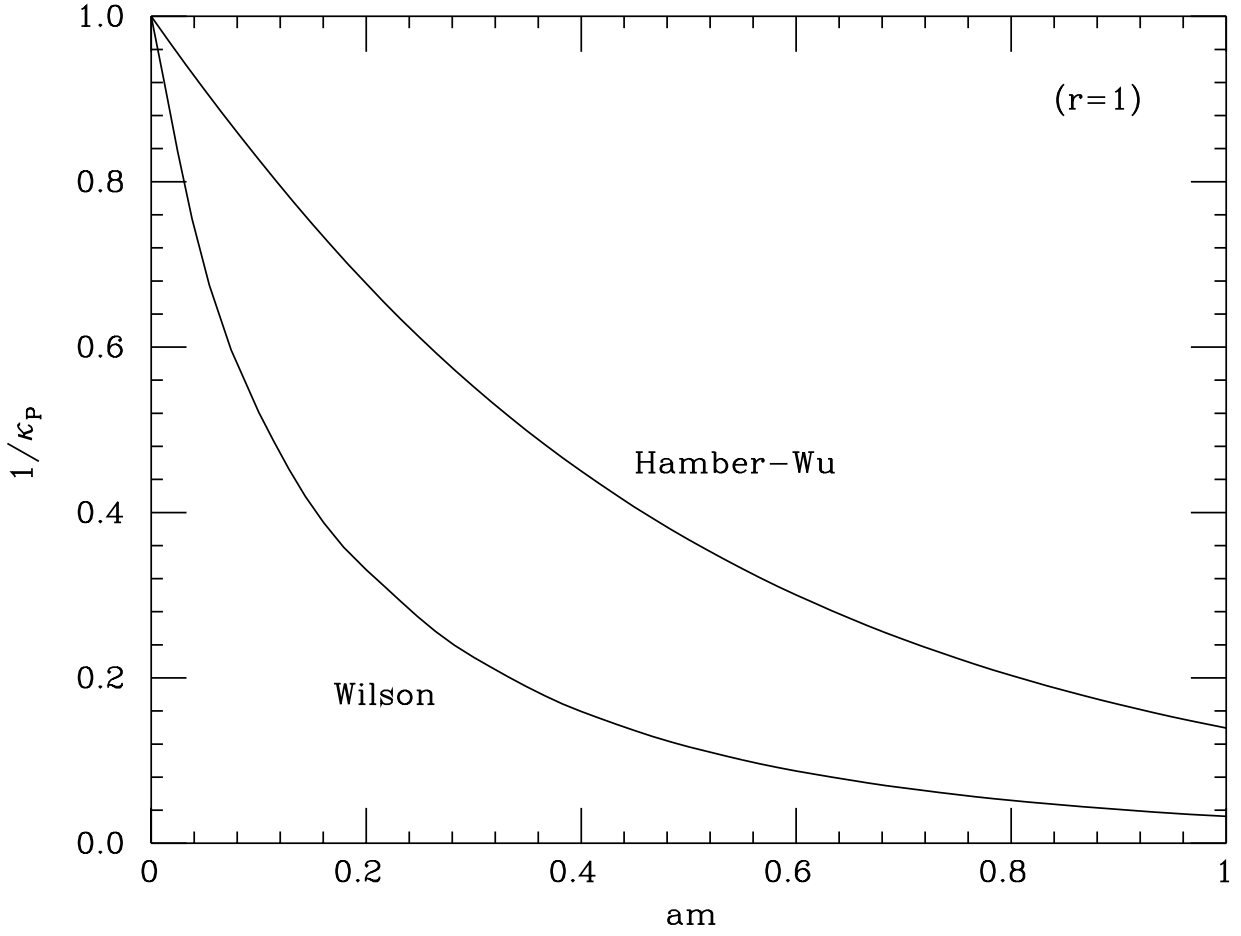


Fig. 4

This figure "fig1-5.png" is available in "png" format from:

<http://arxiv.org/ps/hep-lat/9501007v1>

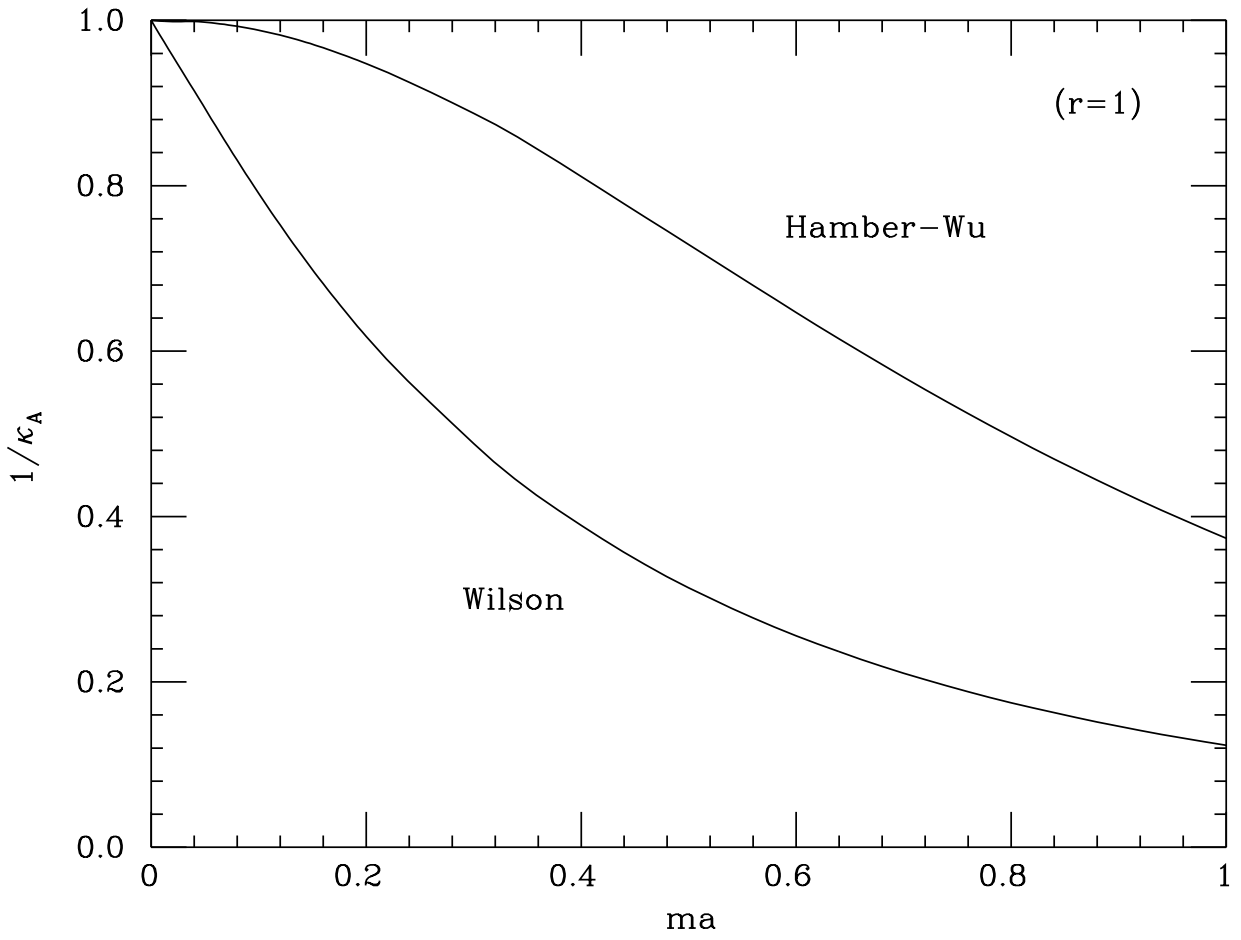


Fig. 5

This figure "fig1-6.png" is available in "png" format from:

<http://arxiv.org/ps/hep-lat/9501007v1>

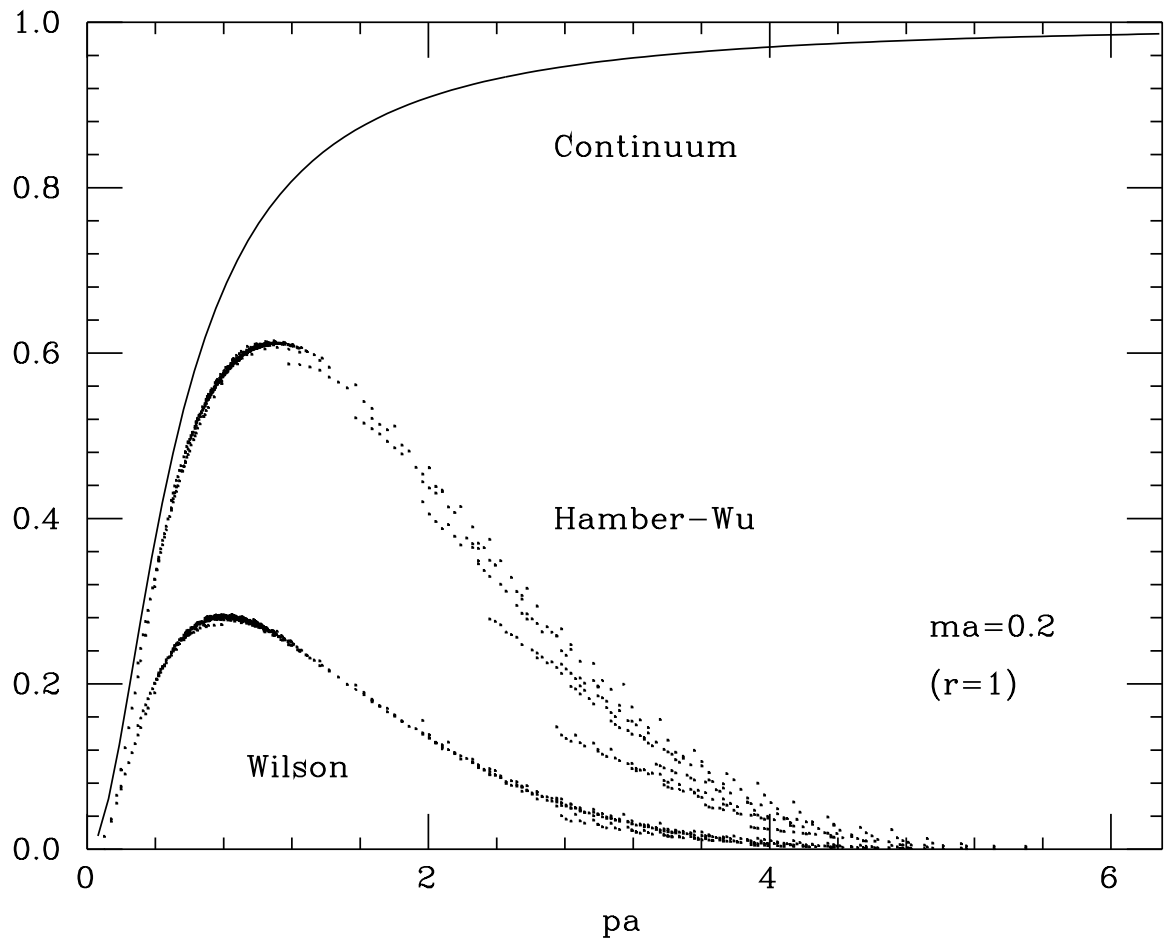


Fig. 6

This figure "fig1-7.png" is available in "png" format from:

<http://arxiv.org/ps/hep-lat/9501007v1>

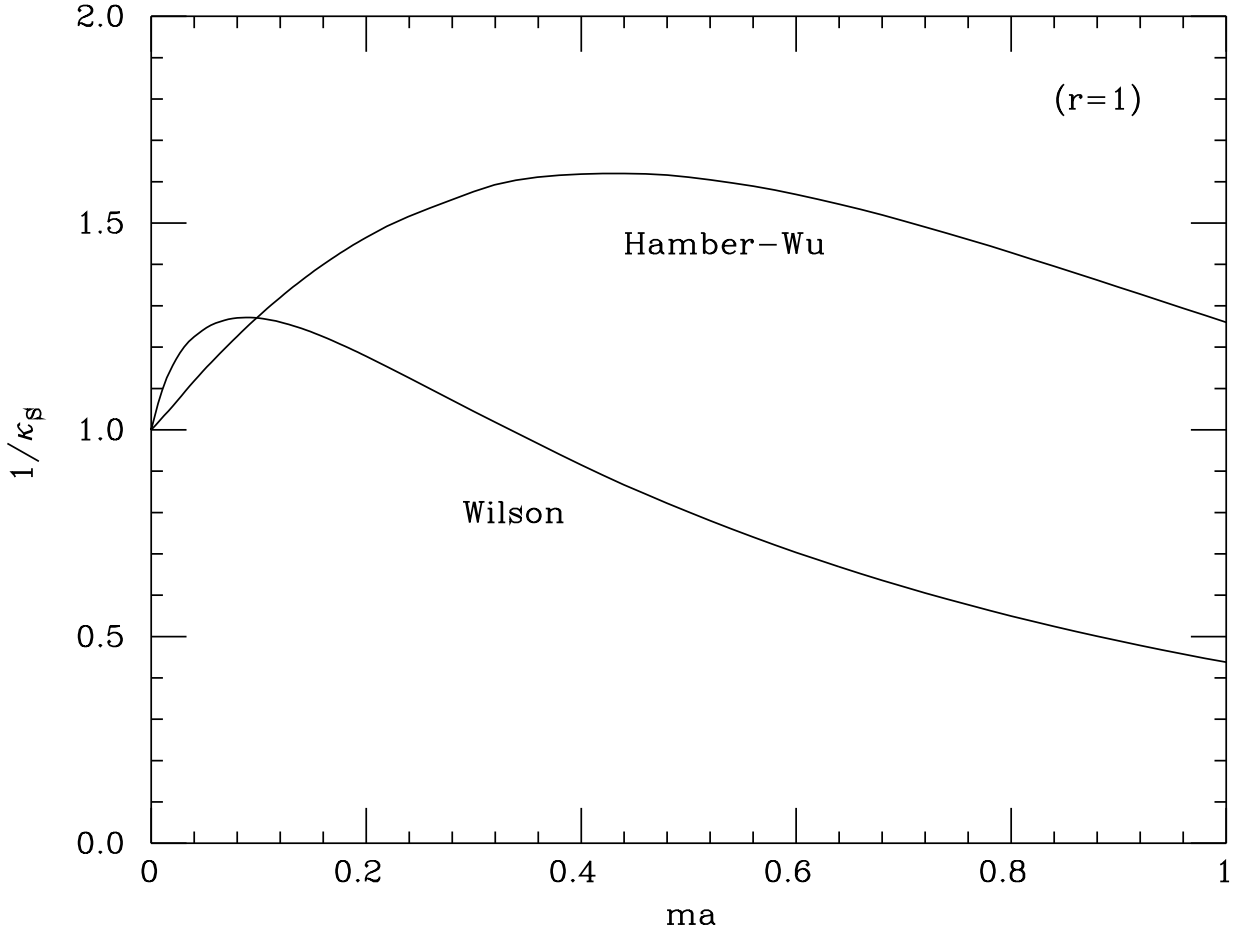


Fig. 7

This figure "fig1-8.png" is available in "png" format from:

<http://arxiv.org/ps/hep-lat/9501007v1>

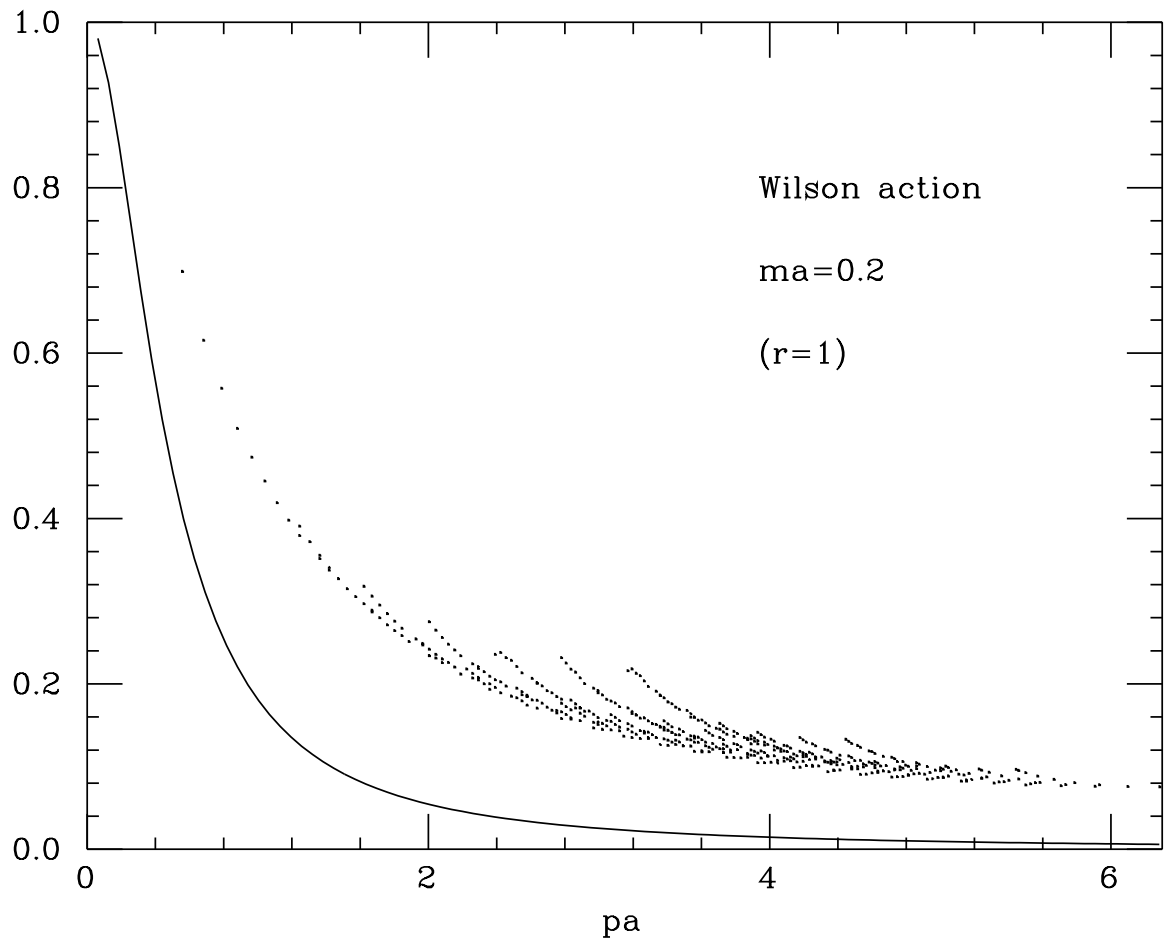


Fig. 8

This figure "fig1-9.png" is available in "png" format from:

<http://arxiv.org/ps/hep-lat/9501007v1>

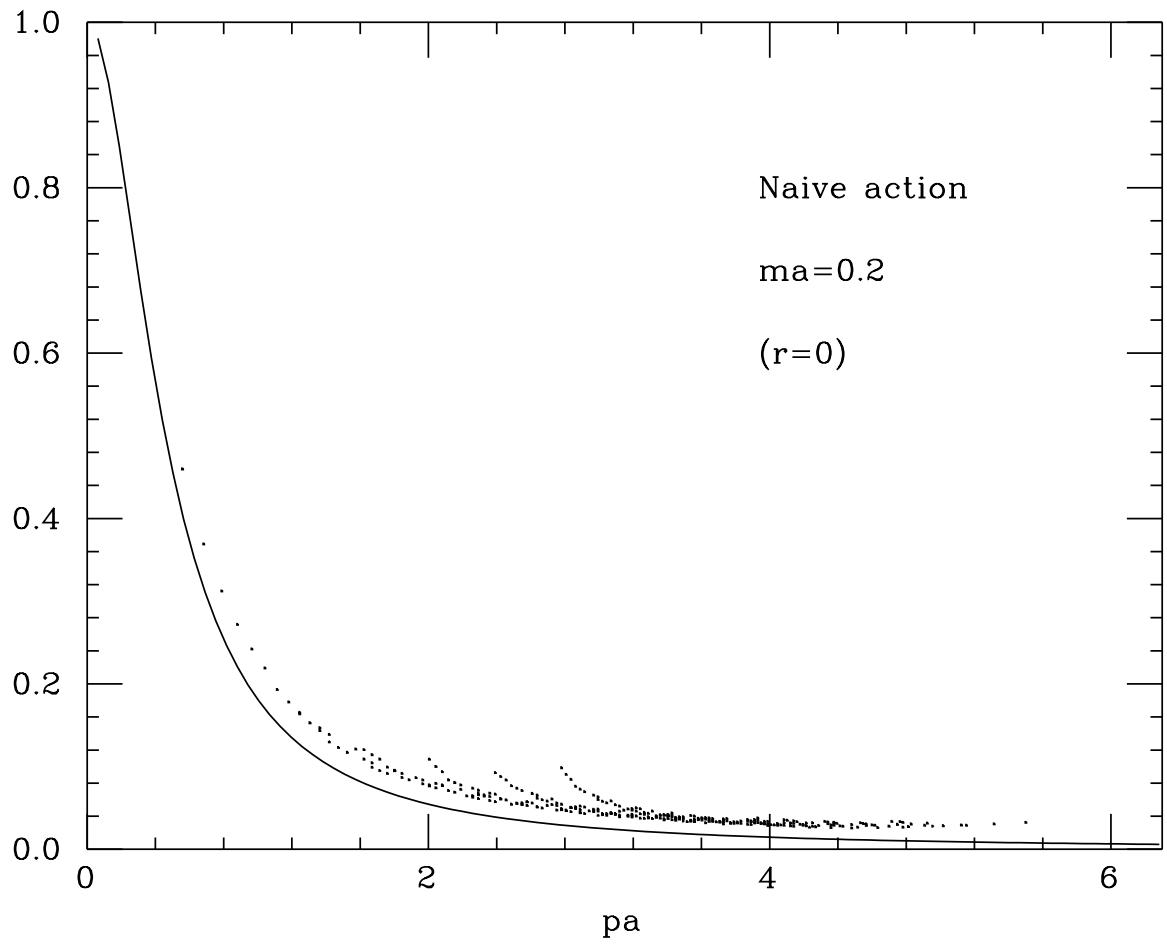


Fig. 9

This figure "fig1-10.png" is available in "png" format from:

<http://arxiv.org/ps/hep-lat/9501007v1>

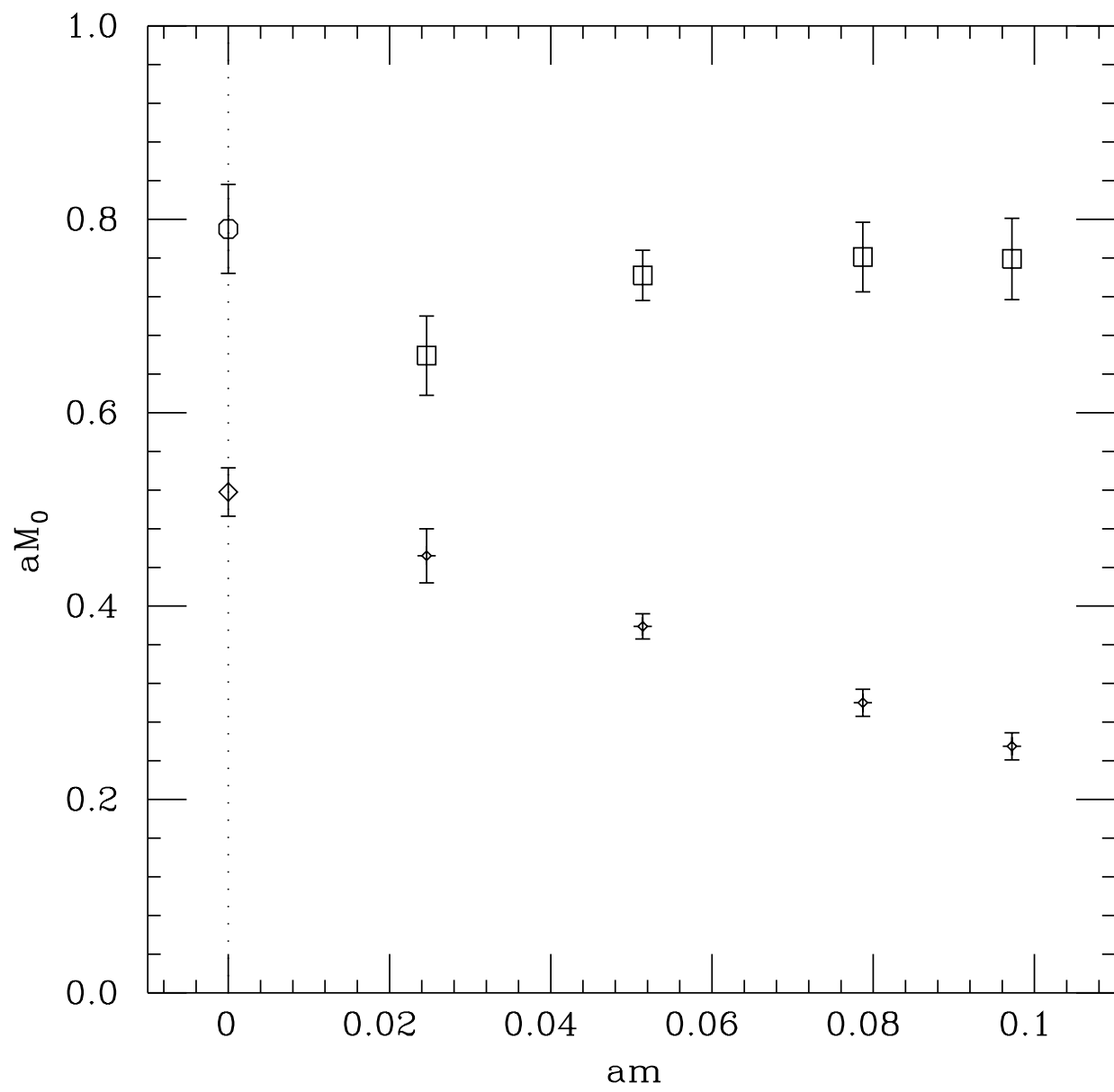
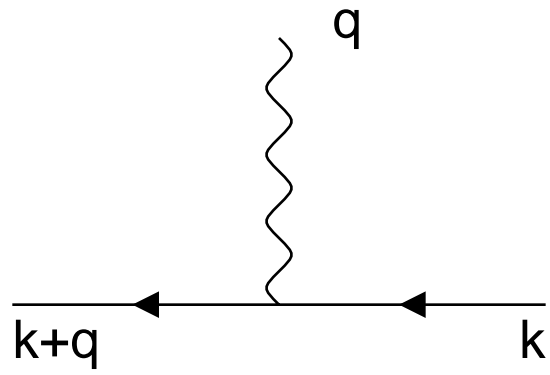


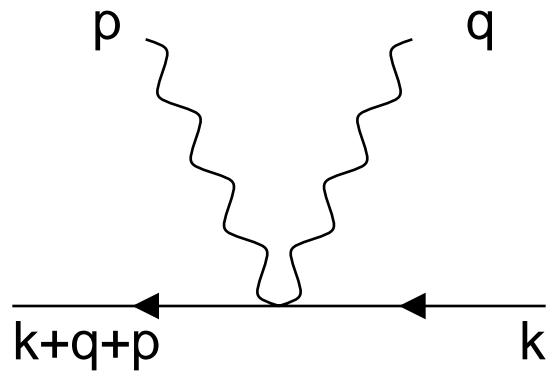
Fig. 10

This figure "fig1-11.png" is available in "png" format from:

<http://arxiv.org/ps/hep-lat/9501007v1>



(a)



(b)

Fig. 11